



## Original article

## Dual stratification effects on double-diffusive convective heat and mass transfer of a sheet-driven micropolar fluid flow

G. Sarojamma<sup>a,\*</sup>, R. Vijaya Lakshmi<sup>a</sup>, K. Sreelakshmi<sup>a</sup>, K. Vajravelu<sup>b</sup><sup>a</sup> Department of Applied Mathematics, Sri Padmavati Mahila University, Tirupati, Andhra Pradesh 517502, India<sup>b</sup> Department of Mathematics, University of Central Florida, Orlando, FL 32816, USA

## ARTICLE INFO

## Article history:

Received 22 April 2018

Accepted 24 May 2018

Available online 5 June 2018

## Keywords:

Dual stratification

Double diffusion

Nonlinear thermal radiation

Second order velocity

Micropolar fluid

## ABSTRACT

The intent of this study is to analyse the influence of nonlinear thermal radiation, thermophoresis, second order slip and magnetic field on the doubly stratified flow of a non-Newtonian micropolar fluid induced by a stretched sheet along with transport of thermal energy and mass species. The radiative heat flux term is modified using the non-linear Rosseland diffusion approximation. The partial differential equations governing the physics of the problem are recast into a set of coupled non-linear ordinary differential equations by using appropriate similarity transformations and later they are solved numerically using RKF-45 algorithm along with shooting technique. Results of the numerical solution are illustrated graphically for several sets of values of the governing parameters. Comparison of our results with the available results in literature for some special cases reveals close agreements. The results indicate that material parameter boosts the velocity and micro-rotation. The temperature ratio parameters that arise due to non-linear thermal radiation are seen to have opposite effect on temperature. It is seen that for strong thermal stratification reverse flow takes place accompanied by an undershoot in temperature. Excessive mass stratification and weaker molecular diffusivity resulted in a significant undershoot of species concentration.

© 2018 The Authors. Production and hosting by Elsevier B.V. on behalf of King Saud University. This is an open access article under the CC BY-NC-ND license (<http://creativecommons.org/licenses/by-nc-nd/4.0/>).

## 1. Introduction

Investigations on fluid flows due to stretching or shrinking sheets are abundantly made by several researchers due to their pragmatic applications in many engineering industries like paper and glass manufacture, extrusion of polymer sheets and wires, drawing of plastic films, spinning of fibres, crystal growing etc. Following the pioneering investigations of Sakiadis (1961) and Crane (1970), several aspects of flow properties with Newtonian and non-Newtonian fluids have been studied. Micropolar fluid is one of the non-Newtonian fluids widely used to model the exotic lubricants, animal blood, polymeric liquids etc. Application of micropolar theory is increasing in various scientific areas. Some of them are

the study of lubricating fluids in bearings, technology of drilling fluids in oil industry, analysis of some polymer suspensions, colloidal solutions and some complicated biological structures in biomedical sciences (see for details, Eluhu and Majumdar, 1998). In the industrial production of polymer solutions and colloidal suspensions, it is pertinent to note the local velocity of the liquid contains a symmetric tensor and microrotation of particles is zero. Some fluids consist of microstructure and belong to a class of fluids with nonsymmetric stress tensor. This type of fluids possess randomly oriented rigid particles suspended in a viscous medium (Lukaszewicz, 1999). Micropolar fluids can support couple stress and body couples. Eringen (1966) developed the theory to describe these micropolar fluids. Animasaun (2017) explored the behavior of melting heat transfer in a stagnation point flow of a micropolar fluid considering the variable properties of viscosity and thermal conductivity of the fluid. Animasaun and Koriko (2017) obtained a new similarity solution to the problem of micropolar fluid flow over an upper horizontal surface of a paraboloid of revolution, which models the flow over a bonnet of a car or a pointed surface of an aircraft, during the homogeneous heterogeneous quadratic auto catalytic chemical reaction.

\* Corresponding author.

E-mail addresses: [gsarojamma@gmail.com](mailto:gsarojamma@gmail.com) (G. Sarojamma), [kuppalapalle.vajravelu@ucf.edu](mailto:kuppalapalle.vajravelu@ucf.edu) (K. Vajravelu).

Peer review under responsibility of King Saud University.



Production and hosting by Elsevier

**Nomenclature**

$a$	constant of dimension (time) <sup>-1</sup>	$Q$	heat source/sink parameter
$A, B$	positive slip constants (m)	$q_r$	radiative heat flux ( $W m^{-2}$ )
$B_0$	magnetic field of strength ( $Wb m^{-2}$ )	$q_w$	surface heat flux ( $W m^{-2}$ )
$C$	concentration of fluid ( $kg m^{-3}$ )	$Q_0$	heat generation/absorption coefficient
$C_f$	skin friction coefficient	$Re_x$	local Reynolds number
$C_0$	reference concentration ( $kg m^{-3}$ )	$Sc$	Schmidt number
$C_w$	concentration at wall ( $kg m^{-3}$ )	$Sh_x$	Sherwood number
$C_\infty$	ambient concentration ( $kg m^{-3}$ )	$T$	temperature of fluid ( $K$ )
$c_p$	specific heat at constant pressure ( $J kg^{-1} K^{-1}$ )	$T_0$	reference temperature ( $K$ )
$D$	mass diffusivity ( $m^2 s^{-1}$ )	$T_w$	temperature at wall ( $K$ )
$Gr$	thermal Grashof number	$T_\infty$	ambient temperature ( $K$ )
$Gc$	solulal Grashof number	$T_{ref}$	reference temperature
$f$	dimensionless stream function	$V_T$	thermophoresis velocity
$g$	acceleration due to gravity ( $m s^{-2}$ )	$(u, v)$	velocity components ( $m s^{-1}$ )
$h$	microrotation function	$u_w$	stretching velocity ( $m s^{-1}$ )
$h_1$	first order velocity Slip parameter	$(x, y)$	coordinate axes (m)
$h_2$	second order velocity Slip parameter	$\alpha$	momentum accommodation coefficient
$j$	micro-inertia density ( $m^2$ )	$\beta$	material parameter
$K$	thermal conductivity of the fluid ( $W m^{-1} K$ )	$\beta_C$	coefficient of concentration expansion ( $kg^{-1} m^3$ )
$K_n$	Knudsen number	$\beta_T$	coefficient of thermal expansion ( $K^{-1}$ )
$k$	vortex viscosity (Pas)	$\gamma$	chemical reaction parameter
$k_0$	chemical reaction	$\varepsilon_1$	thermal stratified parameter
$k^*$	Rosseland mean absorption coefficient ( $m^{-1}$ )	$\varepsilon_2$	solulal stratified parameter
$k_{T,V}$	thermophoretic diffusivity	$\eta$	dimensionless similarity variable
$l$	$\min\left[\frac{1}{K_n}, 1\right]$	$\theta$	dimensionless temperature
$M$	magnetic parameter	$\theta_r, \theta_s$	temperature ratio parameters
$m_1, m_2$	dimensional constants ( $K m^{-1}$ )	$\lambda$	molecular mean free path (m)
$m_x$	wall couple stress	$\mu$	dynamic viscosity ( $kg m^{-1} s^{-1}$ )
$M_w$	dimensionless wall couple stress	$\nu$	kinematic viscosity ( $m^2 s^{-1}$ )
$m_w$	mass flux ( $kg s^{-1} m^{-2}$ )	$\rho$	fluid density ( $kg m^{-3}$ )
$N$	microrotation or angular velocity ( $s^{-1}$ )	$\sigma^*$	Stefan-Boltzman constant ( $W m^{-2} K^{-4}$ )
$Nr$	thermal radiation parameter	$\sigma$	electrical conductivity
$Nu_x$	local Nusselt number	$\tau$	thermophoretic parameter
$n$	boundary parameter	$\tau_w$	wall shear stress (Pa)
$n_1, n_2$	dimensional constants ( $kg m^{-2}$ )	$\phi$	dimensionless concentration
$Pr$	Prandtl number	$\Omega$	spin-gradient viscosity ( $kg m s^{-1}$ )

In the recent past, micro-scale fluid dynamics in the micro-electro-mechanical systems has become a hot topic of research interest. In view of the micro-scale dimensions, behaviour of fluid flow belongs to the slip flow region and differs considerably from the conventional no slip flow (Gal-el-Hak, 1999). Nevertheless, the flow in the slip region conforms the Navier-Stokes equations with slip boundary conditions (Shidlovskiy, 1967; Pande and Goudas, 1996). Further, partial slips are common in flows over moving surfaces pertaining to fluids such as emulsions, suspensions, polymer solutions and foams (Yoshimura and Prudhomme, 1988). Due to wall slip, the behaviour of the fluid and shear stress in the problem differ significantly from that of the flow with no-slip condition. Problems on slip flows under different conditions and configurations have been investigated (Wang, 2002; Fang et al., 2009; Sahoo and Do, 2010; Aurangzaib et al., 2016). Ghosh et al. (2014a) explored the linear stability characteristics of pressure driven miscible two-fluid flow with in a channel with wall slip effects. In a subsequent paper (Ghosh et al., 2014b) they discussed the stability analysis on the two-fluid three layer channel flow considering slip effects and double-diffusive phenomenon. Geetanjali et al. (2017) analysed the stability characteristics of a miscible two-fluid flow in a pipe with wall slip. Karimipour et al. (2017) examined the effects of slip velocity and temperature jump on the MHD nano fluid flow in a microchannel considering  $Al_2O_3$

and Ag as nanoparticles. In these studies, only first-order slip conditions are considered. Second order slip velocity model proposed by Wu (2008) agreed better with the results of Fukui and Kaneko (1990) based on the direct numerical similarities of the linearised Boltzmann equation. Flow behaviour taking the new slip model is seen to be different from the flow with first order slip velocity (Fang et al., 2010). Rosca and Pop (2013) obtained flow velocity and temperature distributions to analyse the wall slip of order two in a steady flow over a permeable surface of stretching/shrinking. They reported that the effect of two slip parameters reduced the surface drag force. Ibrahim (2017) investigated the micropolar fluid flow over a sheet of stretching taking the effects of magnetic field and second order slip into account and remarked that the two parameters of slip incremented the drag coefficient.

When the temperature variation between a surface and the ambient fluid is large radiative heat transfer effects will be significant. Further, at very high operating temperature, the structure of boundary layer and heat transfer rates are varied. Hence, knowledge of radiative thermal energy mechanism will be essential to deal with these processes involving very high temperatures. Some of the examples include nuclear power plants, satellites etc. (Abo-Eldahab and Azzam, 2005). Many studies on radiative heat transfer are available in literature used the linearized form of Rosseland approximation, by considering the temperature differences are

small in the fluid region, which facilitates one to express  $T^4$  as a linear function of temperature. Makinde (2011) examined the interaction of radiative heat transfer, ohmic heating and  $n^{th}$  order homogeneous chemical reaction on the laminar flow of a viscous fluid over a semi infinite permeable plate embedded in a porous medium in the presence of a magnetic field. Shadloo et al. (2013) explored the heat transfer characteristics of flow of a micropolar fluid over a continuous stretching sheet taking the radiative heat transfer. Mabood et al. (2016) investigated the effects of variable thermal conductivity, viscous heating and non-uniform heat generation on the hydromagnetic mixed convective flow of a micropolar fluid in the presence of radiative heat flux and thermo diffusion. Sarojamma et al. (2018) explored the non-orthogonal stagnation point flow and heat transfer of a dual stratified Casson fluid in the presence of radiation. In some situations the temperature difference may not be small. In such situations, while using a non-linear Rosseland diffusion approximation, a new diffusion term arises in the energy transport equation due to the conservation of energy (for details see, Makinde and Annimasau, 2016a, 2016b). When non-linear Rosseland diffusion approximation is used one can deal the problem for small and large differences of the temperature on boundary and the ambient fluid. Consequently the energy equation turns out to be highly non-linear due to the inclusion of non-linear radiative effect. Cortell (2014) reported the numerical results of fluid flow of a viscous fluid due to a stretched surface considering the non-linear radiative heat transfer. Pal and his associates (2017) discussed the impact of non-linear thermal radiation on the MHD heat and mass transfer of a micropolar fluid over a semi infinite plate.

Thermophoresis refers to the migration of small particles from hot surfaces to cold surfaces (Hinds, 1982). It has several applications which include aerosol technology, deposition of radioactive particles in nuclear reactor safety measures and silicon thin film depositions. It is reported that thermophoresis is an effective mechanism for particle collection (Tsai et al., 2004). Hayat and Qasim (2010) addressed the problem of MHD flow, energy and mass transfer over a stretched surface allowing the effects of thermophoresis and Joule heating. Shateyi (2013) reported numerical results investigating the impact of thermophoresis on the MHD flow of a Maxwell fluid past a vertical stretched surface. Mondal and co-researchers (2017) explored the characteristics of velocity, temperature and species concentration viscous fluid flow over a semi infinite permeable inclined flat plate incorporating double diffusive effects.

Stratification pertains to formation of layers due to variation of concentration, temperature differences or the presence of fluids with different densities. Double stratification takes place when both mechanisms of heat and mass occur simultaneously. Study of natural and mixed convection in a doubly stratified medium is of pragmatic significance due to its varied applications. Thermal stratification of oceans and reservoirs, salinity stratification in rivers, estuaries and non-homogeneous mixtures of materials in atmosphere, food processes are a few instances. In the presence of gravitational forces density differences play a vital role on the mechanics and blending of non-homogeneous fluid. For example, temperature stratification in reservoirs inclines to diminish the mixing of oxygen to the bottom water to become anoxic under the action of biological processes. To prevent or predict or solve these type of problems, besides other limnological issues, knowledge of the dynamics of stratified fluids is essential. The concept of stratification is significant in lakes and ponds as it is essential to govern the thermal stratification and concentration differences of hydrogen and oxygen as they may affect the growth rate of all cultured species (Ibrahim and Makinde, 2013). Srinivasacharya and Ram Reddy (2010) investigated the dual stratification on the

transport phenomena by natural convection in a non-Darcy micropolar fluid. In a later study (Srinivasacharya and RamReddy, 2011), they investigated the characteristics pertaining to the transport of momentum, heat and mass of the free convection in a non-Darcy micropolar fluid on the plate admitting dual stratifications and uniform and constant heat and mass fluxes. Ibrahim and Makinde (2013) discussed the effect of double stratification on the boundary layer flow of a nano fluid. Waqas et al. (2017) reported the characteristics of the mixed convective flow of an Oldroyd-B nanofluid taking the effects of heat source and thermal and mass stratifications into account. Hayat et al. (2017a,b) obtained series solutions to address the double stratification effects in a chemically reactive rheological Eyring-Powell liquid flow due to a surface of variable thickness stretching nonlinearly.

Motivated by the above literature and applications, the present analysis explored the energy and mass characteristics of a mixed convective flow of a non-linear radiative micropolar fluid by incorporating the effects of thermophoresis, thermal and solute stratifications and second order wall slip.

### 2. Mathematical formulation

The laminar doubly stratified mixed convective flow of a micropolar fluid induced by a surface of stretching with second order wall slip is proposed. Stretching of the surface is in the x-direction with velocity  $u_w = ax$ , where 'a' is positive constant with dimension per time and y axis perpendicular to the sheet is shown in Fig. 1. A magnetic field of strength  $B_0$  is applied in y-direction.

Governing equations of the flow under investigation reckoning boundary layer approximations are given by (Ibrahim, 2017):

$$\frac{\partial u}{\partial x} + \frac{\partial v}{\partial y} = 0 \tag{1}$$

$$u \frac{\partial u}{\partial x} + v \frac{\partial u}{\partial y} = \frac{(\mu + k)}{\rho} \left( \frac{\partial^2 u}{\partial y^2} \right) + \frac{k}{\rho} \frac{\partial N}{\partial y} - \frac{\sigma B_0^2}{\rho} u + g\beta_T(T - T_\infty) + g\beta_C(C - C_\infty) \tag{2}$$

$$u \frac{\partial N}{\partial x} + v \frac{\partial N}{\partial y} = \frac{\Omega}{\rho j} \frac{\partial^2 N}{\partial y^2} - \frac{k}{\rho j} \left( 2N + \frac{\partial u}{\partial y} \right) \tag{3}$$

$$u \frac{\partial T}{\partial x} + v \frac{\partial T}{\partial y} = \frac{K}{\rho c_p} \frac{\partial^2 T}{\partial y^2} - \frac{1}{\rho c_p} \frac{\partial q_r}{\partial y} + \frac{Q_0}{\rho c_p} (T - T_\infty) \tag{4}$$

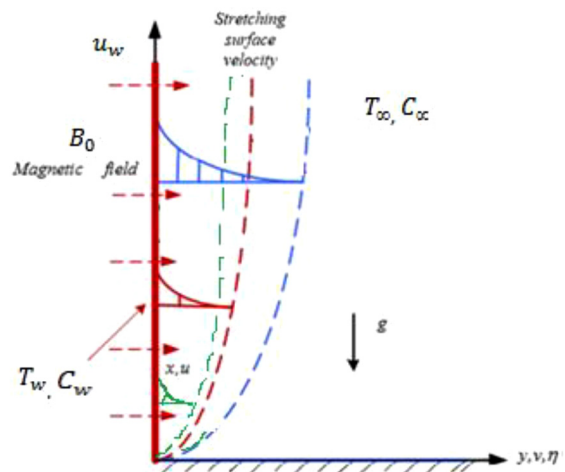


Fig. 1. Physical model and coordinate system.

$$u \frac{\partial C}{\partial x} + v \frac{\partial C}{\partial y} = D \frac{\partial^2 C}{\partial y^2} - k_0(C - C_\infty) - \frac{\partial}{\partial y}(V_T(C - C_\infty)) \quad (5)$$

Using the Rosseland approximation for radiation (Rosseland, 1931), the radiative heat flux is adopted to account for the radiative heat flux as

$$q_r = -\frac{4\sigma^*}{3k^*} \frac{\partial T^4}{\partial y} \quad (6)$$

where  $\sigma^*$  and  $k^*$  are the Stefan-Boltzmann constant and the mean absorption coefficient, respectively. In this study it is assumed that, between any two layers of the fluid flow the temperature differences are not sufficiently small.

At this stage, Eq. (6) introduces a new diffusion term in the Eq. (4) and  $q_r$  takes the form (Hayat et al., 2018)

$$q_r = -\frac{16\sigma^*}{3k^*} T^3 \frac{\partial T}{\partial y} \quad (7)$$

In view to Eq. (7), Eq. (4) reduces to

$$u \frac{\partial T}{\partial x} + v \frac{\partial T}{\partial y} = \frac{K}{\rho c_p} \frac{\partial^2 T}{\partial y^2} + \frac{16\sigma^*}{3k^* \rho c_p} T^3 \frac{\partial T}{\partial y} + \frac{Q_0}{\rho c_p} (T - T_\infty) \quad (8)$$

The boundary conditions are:

$$u = u_w + U_{slip}, v = 0, N = -n \frac{\partial u}{\partial y}, \quad (9)$$

$$T = T_w = T_0 + m_1 x, C = C_w = C_0 + n_1 x \text{ at } y = 0$$

$$u \rightarrow 0, N \rightarrow 0, T \rightarrow T_\infty = T_0 + m_2 x, C \rightarrow C_\infty = C_0 + n_2 x \text{ as } y \rightarrow \infty \quad (10)$$

Following Wu (2008), slip velocity at the surface  $U_{slip}$  is given by

$$U_{slip} = \frac{2}{3} \left( \frac{3 - \alpha l^3}{\alpha} - \frac{3}{2} \frac{(1 - l^2)}{K_n} \right) \lambda \frac{\partial u}{\partial y} - \frac{1}{4} \left( l^4 + \frac{2}{K_n^2} (1 - l^2) \right) \lambda^2 \frac{\partial^2 u}{\partial y^2} \text{ or } U_{slip} = A \frac{\partial u}{\partial y} - B \frac{\partial^2 u}{\partial y^2} \quad (11)$$

Following Talbot et al. (1980) thermophoretic velocity  $V_T$  of the colloidal particles in the fluid, which appears in Eq. (5), is expressed as  $V_T = -\frac{k_t v}{T_{ref}} \frac{\partial T}{\partial y}$ , where  $k_t v$  is the thermophoretic coefficient whose values range from 0.2 to 1.2 as mentioned by Batchelor and Shen (1985).

For any given value of  $K_n$ , it is noticed that  $0 \leq l \leq 1$  (Ibrahim, 2017). The spin gradient viscosity  $\Omega$ , which defines the relationship between the coefficient of viscosity and microinertia  $j$ , is defined as  $\Omega = (\mu + \frac{k}{2})j = \mu(1 + \frac{\beta}{2})j$ , (Mabood et al., 2016), where  $\beta = k/\mu (> 0)$  is the material parameter, which arises due to the microrotation of the fluid molecules. Therefore  $\beta$  symbolises the coupling between Newtonian and rotational viscosities.  $k \rightarrow 0$  as  $\beta \rightarrow 0$ , which corresponds to the case of Newtonian fluid and  $n$  is boundary parameter which is a constant such that  $0 \leq n \leq 1$ .

### 3. Method of solution

Invocation of the following similarity transformations (Hayat et al., 2017a,b, Waqas et al., 2017) facilitates the solution of Eqs. (2)–(5):

$$\eta = \sqrt{\frac{a}{\nu}} y, u = axf', v = -\sqrt{av}f, N = ax\sqrt{\frac{a}{\nu}} h(\eta) \quad (12)$$

$$\theta(\eta) = \frac{T - T_\infty}{T_w - T_0}, \phi(\eta) = \frac{C - C_\infty}{C_w - C_0} \quad (13)$$

Using these similarity transformation and dimensionless variables, the Eqs. (2)–(5) are reduced into the following ordinary non linear differential equations:

$$(1 + \beta)f''' + f f'' - f'^2 + \beta h' - Mf' + Gr\theta + Gc\phi = 0 \quad (14)$$

$$\left(1 + \frac{\beta}{2}\right)h'' - \beta(2h + f'') + fh' - f'h = 0 \quad (15)$$

$$\begin{aligned} \theta'' + Nr \left[ (1 + (\theta_r - \theta_s)\theta)^3 \right] \theta'' \\ + 3Nr \left[ (\theta_r - \theta_s)(1 + (\theta_r - \theta_s)\theta)^2 \right] \theta'^2 \\ + Pr(f\theta' - f'\theta - \varepsilon_1 f' + Q\theta) = 0 \end{aligned} \quad (16)$$

$$\phi'' + Sc(f\phi' - f'\phi - \varepsilon_2 f' - \gamma\phi - \tau(\theta'\phi' + \theta''\phi)) = 0 \quad (17)$$

with boundary conditions:

$$\begin{aligned} f(0) = 0, f'(0) = 1 + h_1 f''(0) + h_2 f'''(0), h(0) = -\eta f''(0), \\ \theta(0) = 1 - \varepsilon_1, \phi(0) = 1 - \varepsilon_2 \end{aligned} \quad (18)$$

$$f'(\eta) \rightarrow 0, h(\eta) \rightarrow 0, \theta(\eta) \rightarrow 0, \phi(\eta) \rightarrow 0 \text{ as } \eta \rightarrow \infty \quad (19)$$

The dimensionless parameters appearing in (14)–(19) are:

$$\begin{aligned} M = \frac{\sigma B_0^2}{\rho a}, Gr = \frac{g\beta_T \Delta T}{a u_w}, Gc = \frac{g\beta_C \Delta C}{a u_w}, Pr = \frac{\rho c_p \nu}{K}, Nr = \frac{16\sigma^* T_\infty^3}{3Kk^*}, \\ \theta_r = \frac{T_w}{T_\infty}, \theta_s = \frac{T_0}{T_\infty}, Q = \frac{Q_0}{\rho c_p a}, \varepsilon_1 = \frac{m_2}{m_1}, \varepsilon_2 = \frac{n_2}{n_1}, Sc = \frac{\nu}{D}, \gamma = \frac{k_0}{a}, \\ h_1 = A\sqrt{\frac{a}{\nu}}, h_2 = -\frac{Ba}{\nu}, \tau = -\frac{k_t(T_w - T_\infty)}{T_r}. \end{aligned}$$

Physical quantities of engineering importance, i.e., surface drag coefficient, the dimensionless wall couple stress, rates of thermal energy and solute transfer are defined by

$$C_f = \frac{\tau_w}{\rho u_w^2}, M_w = \frac{m_x}{\rho x u_w^2}, Nu_x = \frac{x q_w}{K(T_w - T_\infty)}, Sh_x = \frac{x m_w}{D(C_w - C_\infty)} \quad (20)$$

where the wall shear stress  $\tau_w$ , the wall couple stress  $m_x$ , the surface heat flux  $q_w$  and mass flux  $m_w$  are given by

$$\begin{aligned} \tau_w = \left( (\mu + k) \frac{\partial u}{\partial y} + kN \right)_{y=0}, m_x = \Omega \left( \frac{\partial N}{\partial y} \right)_{y=0}, \\ q_w = -K \left( 1 + \frac{16\sigma^* T^3}{3Kk^*} \right) \left( \frac{\partial T}{\partial y} \right)_{y=0}, m_w = -D \left( \frac{\partial C}{\partial y} \right)_{y=0} \end{aligned} \quad (21)$$

Using Eq. (21) in Eq. (20), we obtain

$$C_f \sqrt{Re_x} = -(1 + \beta(1 - n))f''(0) \quad (22)$$

$$M_w Re_x = \left( 1 + \frac{\beta}{2} \right) h'(0) \quad (23)$$

$$Nu_x / \sqrt{Re_x} = -\left( 1 + Nr[1 + (\theta_r - \theta_s)\theta(0)]^3 \right) \left( \frac{1}{1 - \varepsilon_1} \right) \theta'(0) \quad (24)$$

$$Sh_x / \sqrt{Re_x} = -\left( \frac{1}{1 - \varepsilon_2} \right) \phi'(0) \quad (25)$$

where  $Re_x = ax^2/\nu$  is a local Reynolds number.

The ordinary differential equations (14)–(17) are coupled and highly non-linear and exact analytical solutions cannot be determined and are solved together with (18) and (19) using the efficient Runge-Kutta-Fehlberg (RKF-45) algorithm and derived the numerical solutions.

**Table 1**  
Comparison of values of  $-f''(0)$  and  $-\theta'(0)$  with slip factor  $h_1$  and  $Pr$  when  $\beta = M = Gr = Gc = Nr = h_2 = Sc = \gamma = \tau = \varepsilon_1 = \varepsilon_2 = n = 0$ .

$h_1$ ( $Pr = 0$ )	Sahoo and Do (2010) $-f''(0)$	Ibrahim (2017) $-f''(0)$	Present results $-f''(0)$	$Pr$ ( $h_1 = 0$ )	Ishak et al. (2009) $-\theta'(0)$	Present results $-\theta'(0)$
0.0	1.001154	1.000000	1.000000	0.72	0.8086	0.808681
0.5	0.589195	0.591196	0.591196	1.0	1.0000	1.000001
1.0	0.428450	0.430160	0.430160	3.0	1.9237	1.923677
2.0	0.282893	0.283980	0.283981	10.0	3.7207	3.720648
3.0	0.213314	0.214055	0.214056	100.0	12.2941	12.293834

**Table 2**  
Comparison of  $-f''(0)$  with  $M, \beta, h_2$  when  $h_1 = 1, Pr = 1, n = 0.5, Gr = Gc = Nr = Sc = \gamma = \tau = \varepsilon_1 = \varepsilon_2 = 0$ .

$M$	$\beta$	$h_2$	Ibrahim (2017)	Present Results	Error difference
0.1			0.3220	0.32197	0.00003
0.2	0.1	-1	0.3262	0.32620	0.00000
0.4			0.3315	0.33147	0.00003
	1		0.3173	0.31728	0.00002
0.2	2	-1	0.3068	0.30678	0.00000
	3		0.2971	0.29709	0.00001
		-1	0.3068	0.30675	0.00005
0.2	2	-2	0.2588	0.25883	-0.00003
		-3	0.2262	0.22622	-0.00002

The accuracy of our numerical procedure is achieved by collating our results, viz.,  $-f''(0)$  for various first order slip factors  $h_1$  with those of Sahoo and Do (2010) and Ibrahim (2017) when  $\beta = M = Gr = Gc = Pr = Nr = h_2 = Sc = \gamma = \tau = \varepsilon_1 = \varepsilon_2 = n = 0$ . Collation of values of  $-\theta'(0)$  with those evaluated by Ishak et al. (2009) for various values of  $Pr$  in the absence of  $\beta, M, h_1, h_2, n, Gr, Gc, Sc, \gamma, \tau, \varepsilon_1, \varepsilon_2$  presented in Table 1 shows a very close agreement with them. Table 2 shows that  $-f''(0)$  are compared with those evaluated by Ibrahim (2017) in the absence of  $Gr, Gc, Nr, Sc, \gamma, \tau, \varepsilon_1, \varepsilon_2$  for various  $M, \beta, h_2$  and this reveals that our results are very closely agreed.

**4. Results and discussion**

The impact of various physical parameters that emerged in this analysis on the flow variables has been highlighted through graphs and discussed. In the discussion of results  $Pr$  is taken as 0.71 which represents air. The values of  $Sc$  is taken as  $Sc = 0.22, 0.66, 0.94, 1, 2, 2.62$  representing diffusing chemical species of common interest in air for hydrogen, oxygen, carbon dioxide, methanol, ethyl benzene and propyl benzene respectively. The values of

material parameter  $\beta$  used in this study are the same used by Ibrahim (2017).

Fig. 2(a) reveals that the velocity is enhanced significantly via larger values of the material parameter  $\beta$ , as larger  $\beta$  indicates lesser viscosity of the fluid and hence the flow is accelerated. Fig. 2(b) indicates that the microrotation  $h$  shows an initial decay near the boundary and subsequently proceeding further away from the stretching surface the micro-rotation boosts up in the rest of the region. It may be concluded that  $h$  is higher when  $\beta$  is incremented. This is owing to diminution of viscosity of the material which leads to the amelioration of micro-rotation. Fig. 3(a) and (b) represent the plots of velocity and microrotation for a variation in magnetic parameter  $M$ . Lorentz force suppresses the flow with reduced velocities as expected due to the retarding nature of the Lorentz force. Stronger Lorentz force further oppresses the velocity. An initial rise in microrotation near the boundary occurs and later it diminishes. Fig. 4(a) and (b) indicate the variation of thermal buoyancy force ( $Gr$ ) on velocity and microrotation. It is seen that flow accelerates with an increase in the buoyancy parameter  $Gr$  as thermal buoyancy ( $Gr > 0$ ) assists the fluid flow in the boundary layer. At this point, following the analysis of Shah et al. (2018), the slope of linear regression (slp) near the wall for the increase in velocity profile is estimated as 0.104340542146213.  $Gr < 0$  corre-

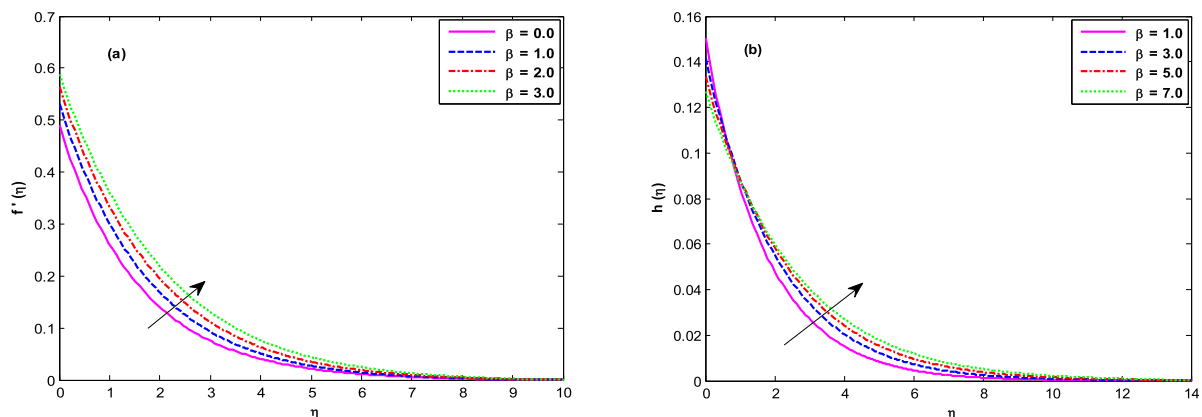


**Fig. 2.** Effect of  $\beta$  on (a) velocity (b) Microrotation when  $M = Nr = \theta_s = Q = \varepsilon_1 = \varepsilon_2 = \gamma = 0.1, \tau = 0.2, Gr = Gc = 0.05, h_1 = 1.0, Pr = 0.71, h_2 = -1.0, \theta_r = 0.2, n = 0.5, Sc = 0.66$ .

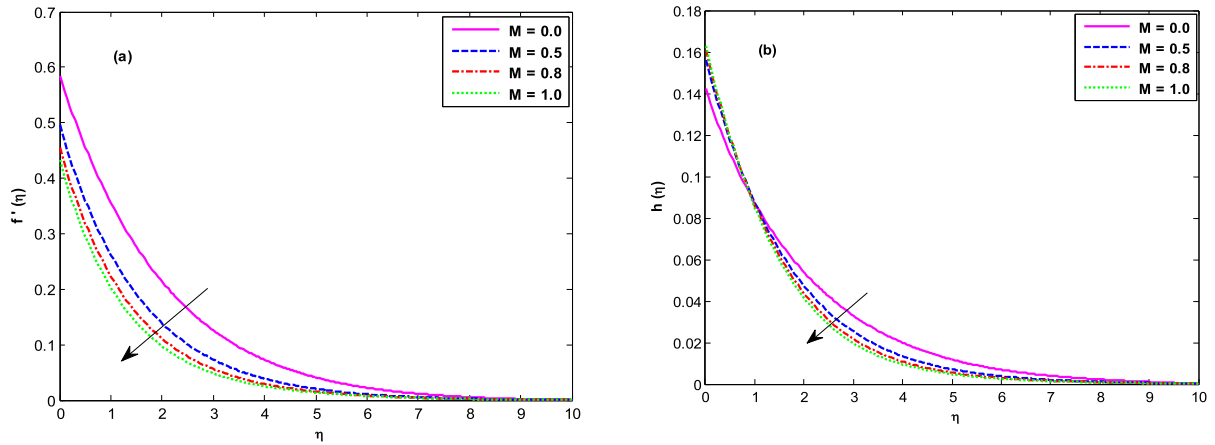


**Fig. 3.** Effect of  $M$  on (a) velocity (b) Microrotation when  $\beta = 2.0$ ,  $Nr = \theta_s = Q = \varepsilon_1 = \varepsilon_2 = \gamma = 0.1$ ,  $\tau = 0.2$ ,  $Gr = Gc = 0.05$ ,  $h_1 = 1.0$ ,  $Pr = 0.71$ ,  $h_2 = -1.0$ ,  $\theta_r = 0.2$ ,  $n = 0.5$ ,  $Sc = 0.66$ .

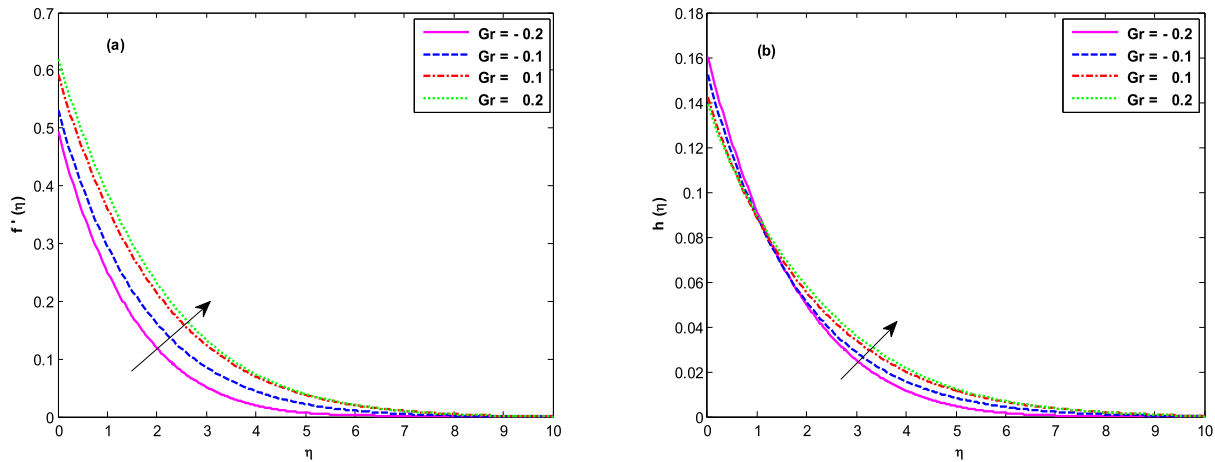


**Fig. 4.** Effect of  $Gr$  on (a) velocity (b) Microrotation when  $\beta = 2$ ,  $M = Nr = \theta_s = Q = \varepsilon_1 = \varepsilon_2 = \gamma = 0.1$ ,  $\tau = 0.2$ ,  $Gc = 0.05$ ,  $h_1 = 1.0$ ,  $Pr = 0.71$ ,  $h_2 = -1.0$ ,  $\theta_r = 0.2$ ,  $n = 0.5$ ,  $Sc = 0.66$ .

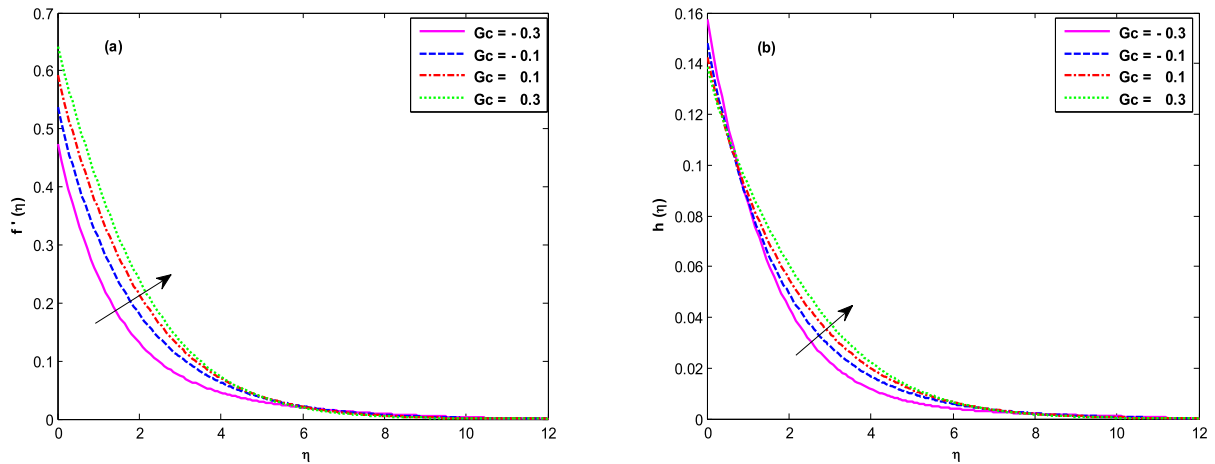


**Fig. 5.** Effect of  $Gc$  on (a) velocity (b) Microrotation when  $\beta = 2$ ,  $M = Nr = \theta_s = Q = \varepsilon_1 = \varepsilon_2 = \gamma = 0.1$ ,  $\tau = 0.2$ ,  $Gr = 0.05$ ,  $h_1 = 1.0$ ,  $Pr = 0.71$ ,  $h_2 = -1.0$ ,  $\theta_r = 0.2$ ,  $n = 0.5$ ,  $Sc = 0.66$ .

sponds to opposing buoyancy that leads to a reduction in velocity. Thus the boundary layers of aiding buoyancy are thicker than those of opposing buoyancy. Microrotation is observed to diminish for an increment in  $Gr$  near the boundary till  $\eta = 1.1$  and later it improves

up to  $\eta = 7$  and eventually attains the free stream velocity. At  $\eta = 0$  the slp for reduction in the profile of microrotation is obtained as  $-0.053439868075764$  and at  $\eta = 3$  the slp is estimated as  $0.01161317616539$ .

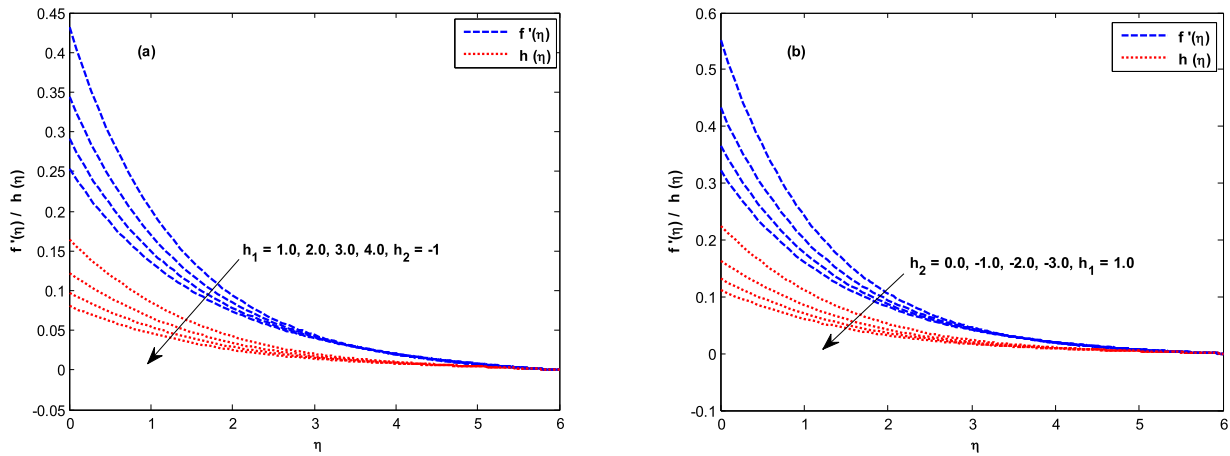


**Fig. 6.** Velocity and Microrotation profiles for (a)  $h_1$  (b)  $h_2$  when  $\beta = 2, M = Nr = \theta_s = Q = \varepsilon_1 = \varepsilon_2 = \gamma = 0.1, \tau = 0.2, Gr = Gc = 0.05, Pr = 0.71, \theta_r = 0.2, n = 0.5, Sc = 0.66$ .

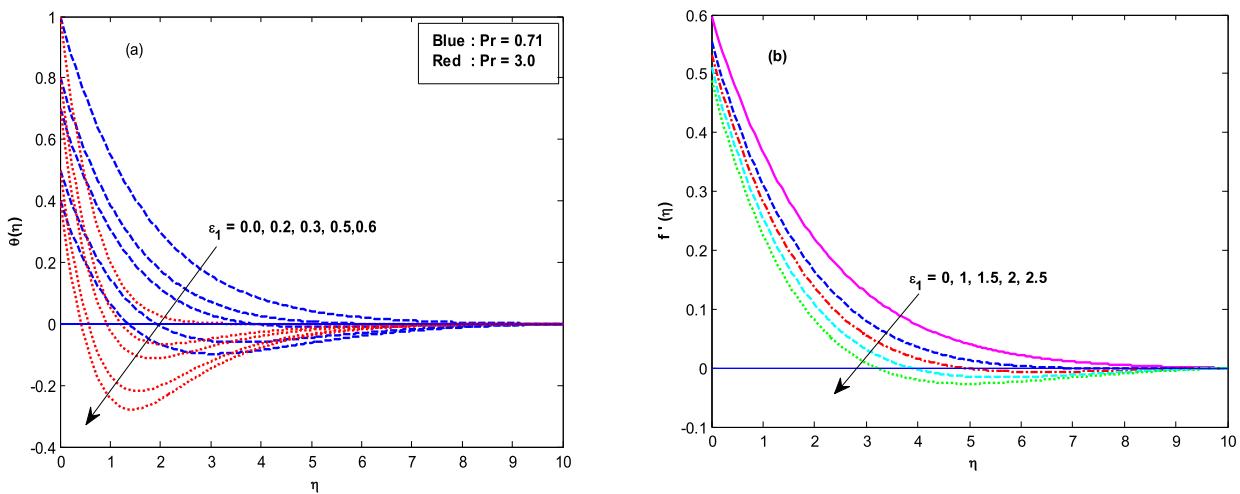
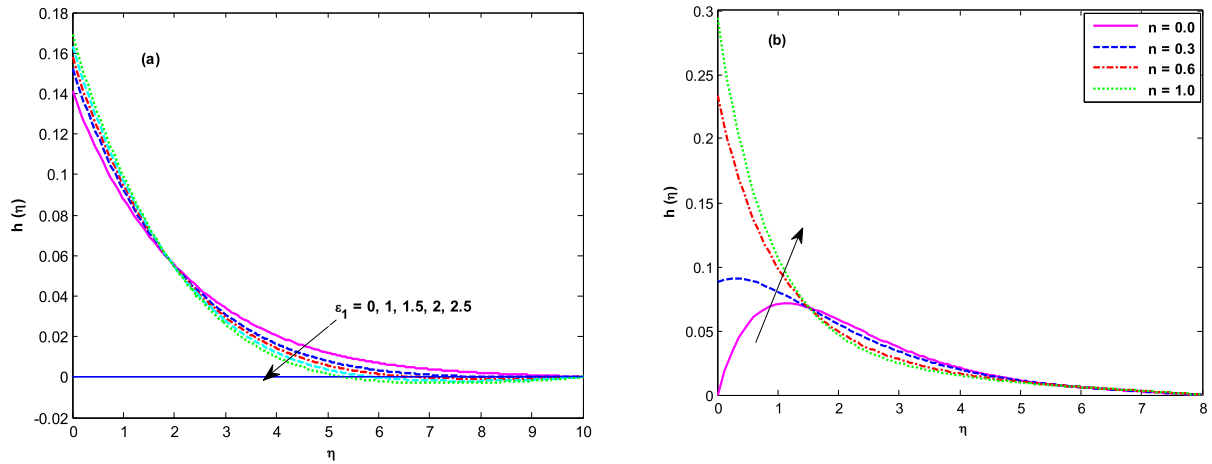


**Fig. 7.** Effect of  $\varepsilon_1$  on (a) Temperature (b) velocity when  $\beta = 2, M = Nr = \theta_s = Q = \varepsilon_2 = \gamma = 0.1, \tau = 0.2, Gr = Gc = 0.1, h_1 = 1, Pr = 0.71, h_2 = -1.0, \theta_r = 0.2, n = 0.5, Sc = 0.66$ .

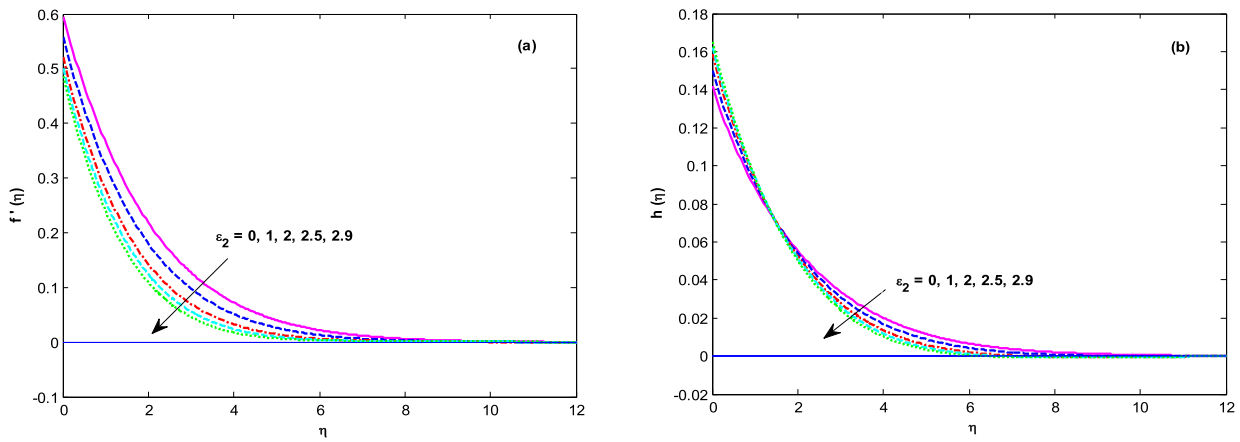
The variation of solutal Grashof number  $Gc$  on velocity, microrotation is represented in Fig. 5(a) and (b). We see that velocity is an increasing function of  $Gc$  as it is the ratio of the force of species buoyancy to viscous force. Microrotation follows a decreasing trend in the vicinity of the boundary up to  $\eta = 0.6$  and afterwards shows an opposite behaviour eventually attaining its free stream condition.

Fig. 6(a) discloses that the first order slip  $h_1$  has a predominant influence on velocity than on microrotation  $h(\eta)$ . Velocity on the boundary is decreased in the range 0.43–0.25 for a variation of  $h_1$  in the range 1.0–4.0 while  $h(\eta)$  changes from 0.16 to 0.08. Fig. 6(b) indicates the relationship between velocity and wall slip of order two in the boundary layer. The velocity curves emanate from higher values prescribed on the boundary. The profile for  $h_2 = 0$  i.e., in the absence of second order slip, originate from the value 0.552 and decreases rapidly as it moves just a little away from the boundary. As the profile further proceeds, the gradient reduces and is followed by a substantial fall in the velocity till the end of the boundary layer. The curves for  $|h_2| = 1, 2, 3$  adopt a similar trend of large gradient in the vicinity of the boundary, followed by a drop in the slope. Microrotation also shows qualitatively the same trend of the velocity. However, quantitatively the values of microrotation are almost half the values of the velocity.

Fig. 7(a) presents the relationship between temperature in the thermal boundary layer, thermal stratification parameter  $\varepsilon_1$  and Prandtl number  $Pr$ . For higher Prandtl number  $Pr = 3.0$  the temperature gradients are larger near the surface with a substantial drop in temperature due to smaller diffusivity. Temperature is found to decrease with increasing  $\varepsilon_1$  for both small and higher values of  $Pr$  i.e.,  $Pr = 0.71$  and  $Pr = 3.0$ . It is observed there is a small undershoot of temperature or negative temperature away from the boundary when  $Pr = 0.71$  and  $\varepsilon_1 = 0.3$  due to excessive stratification. This undershoot of temperature increases with an increment in  $\varepsilon_1$  and the point of undershoot is skewed towards the surface. When  $Pr = 3.0$ , this undershoot of temperature is seen even for smaller values of  $\varepsilon_1$  and is more significant with a rise in  $\varepsilon_1$  as a result of the cumulative effect of excessive thermal stratification and weaker thermal diffusivity. Physically, the ambient temperature  $T_\infty$  is raised downstream and the flow coming from below tends to have a temperature lower than that of the local temperature and thus the undershoot in temperature results. Fig. 7(b) depicts the relationship between velocity and thermal stratification parameter  $\varepsilon_1$ . It is observed that velocity is suppressed with  $\varepsilon_1$ . It is interesting to note that for larger values of  $\varepsilon_1$ , for  $\varepsilon_1 = 1.5$ , an adverse flow away from the boundary occurs due to the smaller values of buoyancy and hence a



**Fig. 8.** Microrotation profiles for (a)  $\varepsilon_1$  with  $n = 0.5$  (b)  $n$  with  $\varepsilon_1 = 0.1$  when  $\beta = 2, M = Nr = \theta_s = Q = \varepsilon_2 = \gamma = 0.1, \tau = 0.2, Gr = Gc = 0.1, h_1 = 1.0, Pr = 0.71, h_2 = -1.0, \theta_r = 0.2, Sc = 0.66$ .



**Fig. 9.** Effect of  $\varepsilon_2$  on (a) velocity and (b) Microrotation when  $\beta = 2, M = Nr = \theta_s = Q = \varepsilon_1 = \gamma = 0.1, \tau = 0.2, Gr = Gc = 0.1, h_1 = 1.0, Pr = 0.71, h_2 = -1.0, \theta_r = 0.2, n = 0.5, Sc = 0.66$ .

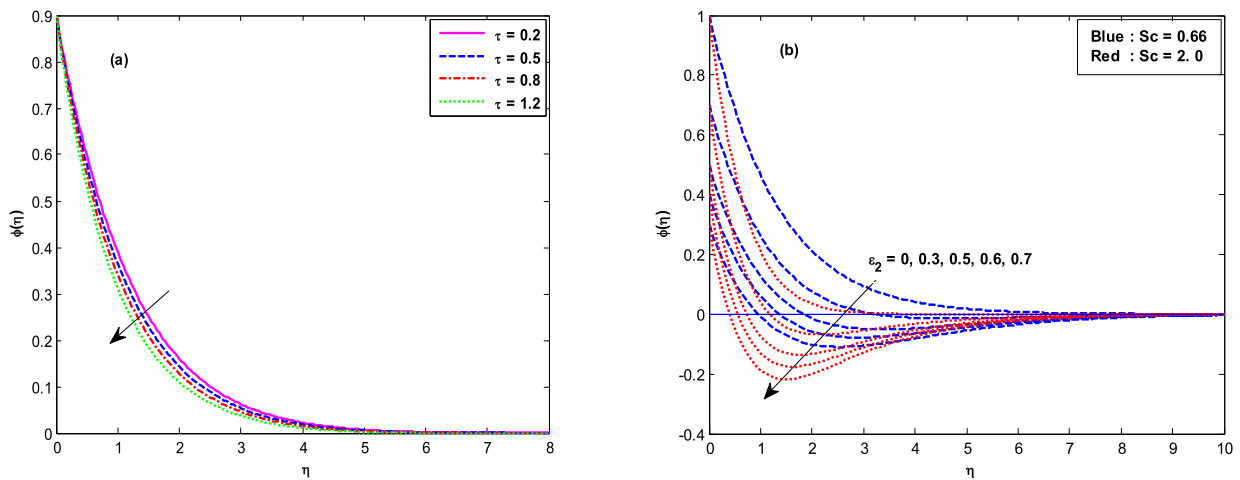


**Fig. 10.** Concentration profiles for (a)  $\tau$  with  $\varepsilon_2 = 0.1$  (b)  $\varepsilon_2$  with  $\tau = 0.2$  when  $\beta = 2, M = Nr = \theta_s = Q = \varepsilon_1 = \gamma = 0.1, Gr = Gc = 0.1, h_1 = 1.0, Pr = 0.71, h_2 = -1.0, \theta_r = 0.2, n = 0.5, Sc = 0.66$ .

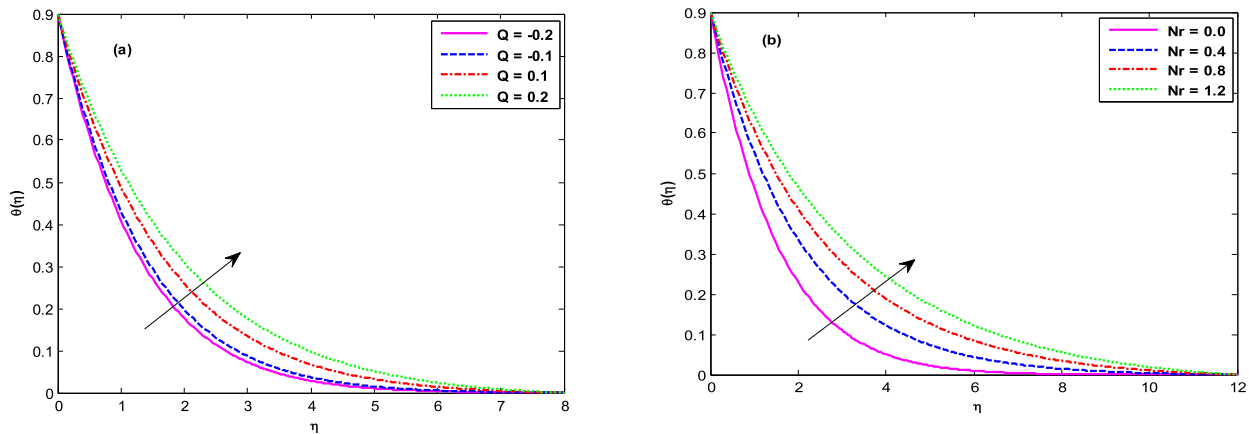


**Fig. 11.** Temperature distribution. (a) Effect of  $Q$  with  $Nr = 0.1$  (b) Effect of  $Nr$  with  $Q = 0.1$  when  $\beta = 2$ ,  $M = \theta_s = \varepsilon_1 = \varepsilon_2 = \gamma = 0.1$ ,  $\tau = 0.2$ ,  $Gr = Gc = 0.05$ ,  $h_1 = 1.0$ ,  $Pr = 0.71$ ,  $h_2 = -1.0$ ,  $\theta_r = 0.2$ ,  $n = 0.5$ ,  $Sc = 0.66$ .

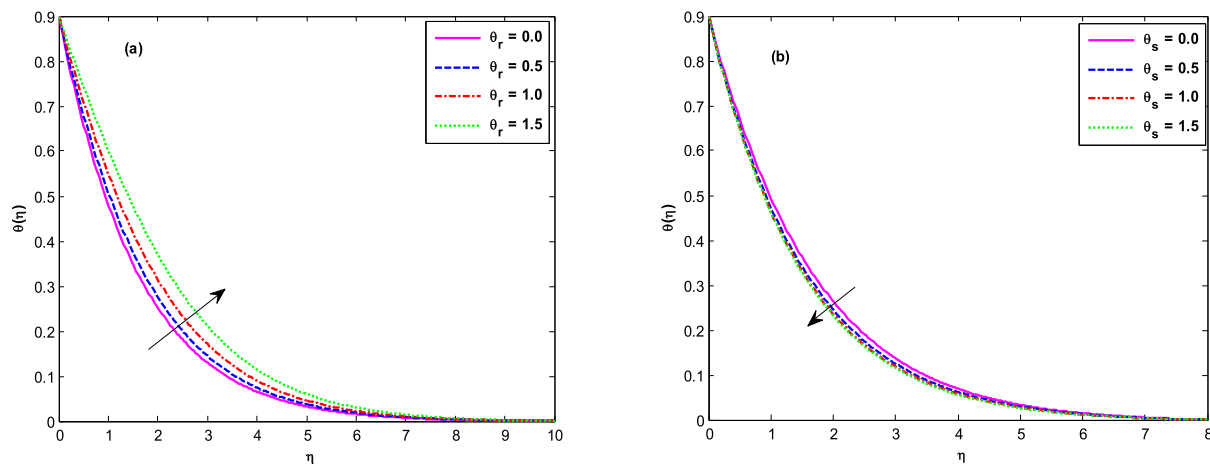


**Fig. 12.** Temperature distribution. (a) Effect of  $\theta_r$  with  $\theta_s = 0.1$  (b) Effect of  $\theta_s$  with  $\theta_r = 0.2$  when  $\beta = 2$ ,  $M = Nr = Q = \varepsilon_1 = \varepsilon_2 = \gamma = 0.1$ ,  $\tau = 0.2$ ,  $Gr = Gc = 0.05$ ,  $h_1 = 1.0$ ,  $Pr = 0.71$ ,  $h_2 = -1.0$ ,  $n = 0.5$ ,  $Sc = 0.66$ .

reverse flow takes place. With higher values of  $\varepsilon_1$  the reverse flow zone expands.

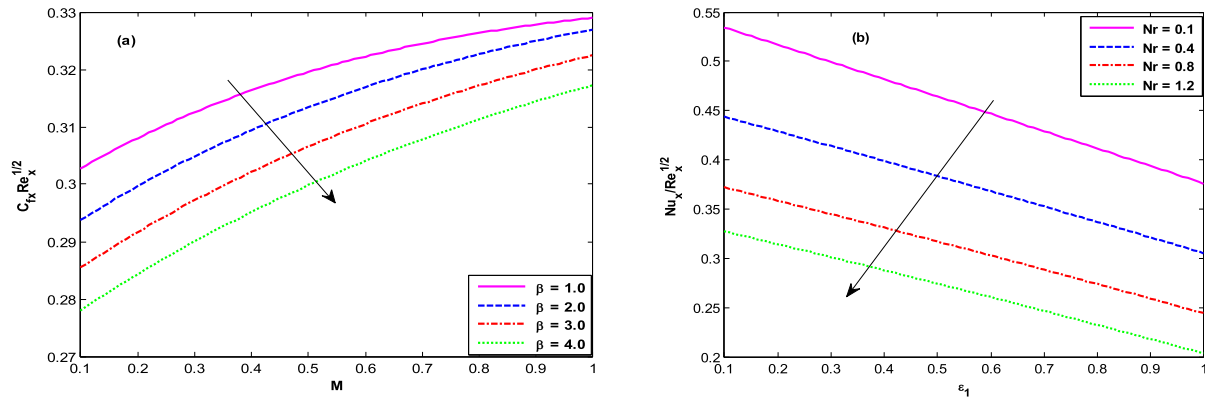
From Fig. 8(a) microrotation is seen to enhance near the boundary up to  $\eta = 1.785$  and subsequently, a reversal trend is noticed for  $\varepsilon_1$ . Fig. 8(b) shows the variation of the boundary parameter. It may be noted that boundary parameter  $n$  varies in the range from 0 to 1. Further, when  $n = 0$  known as strong concentration in which case the microelements close to the wall are unable to rotate. The case  $n = 0.5$  amounts to the disappearance of antisymmetric part of the stress tensor indicating the weak concentration of microelements. The case  $n = 1$  is used for modeling of turbulent boundary layer flow. Microrotation across the flow is found to be an increasing function of parameter  $n$  near the wall. However velocity, temperature and concentration are not displayed for brevity. From Fig. 9(a) velocity is seen to show a reduction in velocity for an increment in  $\varepsilon_2$  as in the case of  $\varepsilon_1$ . The effect of  $\varepsilon_2$  on microrotation is qualitatively exactly similar to that of  $\varepsilon_1$  as shown in Fig. 9(b).

Fig. 10(a) reveals that species concentration of the fluid steadily changes from higher value to the lower value and ultimately satisfies the free stream condition in the mass boundary layer with diluted concentration of the fluid for increasing thermophoresis. Fig. 10(b) presents the relation of species concentration between  $Sc$  and solutal stratification parameter  $\varepsilon_2$ . As the role of  $Sc$  on species concentration is same as that of  $Pr$  on temperature, it is

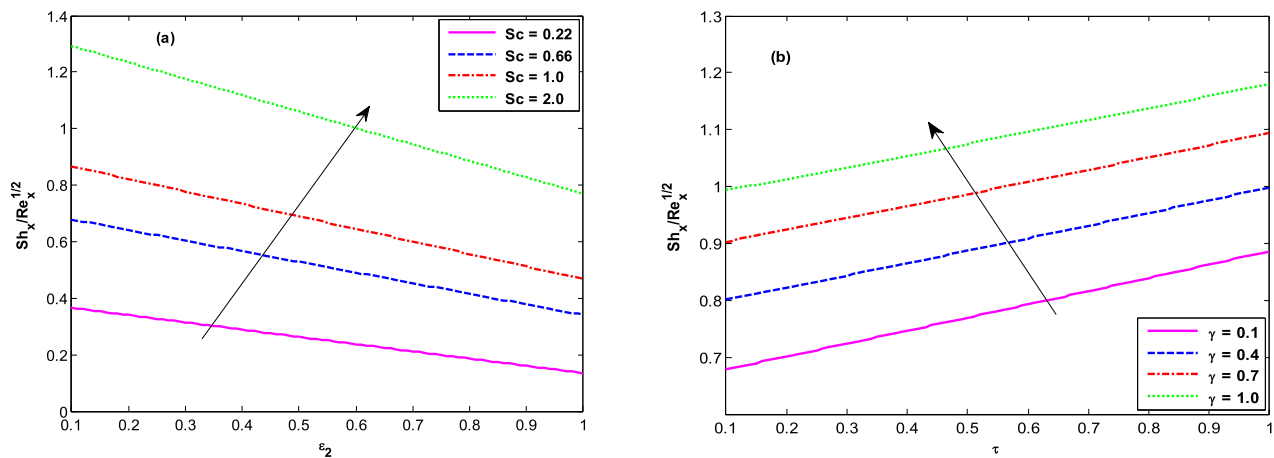
observed that the behaviour of species concentration for a variation of  $Sc$  and  $\varepsilon_2$  is qualitatively similar to that of the temperature with regard to  $Pr$  and  $\varepsilon_1$ .

Fig. 11(a) shows that as the strength of the heat source intensified the temperature is enhanced due to the release of larger thermal energy and a reverse behaviour is noticed in the case of heat sink. Fig. 11(b) indicates that the temperature is significantly enhanced for greater values of thermal radiation parameter  $Nr$ . This can be explained physically, higher values of  $Nr$  facilitate the release of higher thermal energies in the fluid region. The effect of temperature ratio parameters  $\theta_r$  and  $\theta_s$  on temperature field is presented in Fig. 12 and it can be seen that as  $\theta_r$  takes higher values, temperature raises and a reverse trend is noticed with  $\theta_s$ , as  $\theta_s$  has ‘-’ sign: This is justified by Eq. (4).

Fig. 13(a) evinces that the wall drag force grows monotonically with the intensification of strength of the magnetic field and an increment in material parameter reduces the drag force considerably for weaker magnetic fields. Fig. 13(b) depicts that the Nusselt number which represents the rate of heat transfer shows a linear reduction for increasing thermal stratification parameter. Rate of heat transfer shows a diminishing trend for an increment in  $Nr$ . Fig. 14(a) is the plot of mass transfer coefficient ( $Sh$ ) versus solutal stratification parameter for a variation in  $Sc$ . It is evident that  $Sh$  falls linearly with solutal stratification parameter. The effect of Schmidt’s number on the mass transfer coefficient is found to be promisingly



**Fig. 13.** (a)  $C_f$  with  $\beta$  and  $M$  when  $Nr = \varepsilon_1 = 0.1$  (b)  $Nu$  with  $Nr$  and  $\varepsilon_1$  where  $\beta = 2$ ,  $M = 0.1$  when  $\theta_s = Q = \varepsilon_2 = \gamma = 0.1$ ,  $\tau = 0.2$ ,  $Gr = Gc = 0.05$ ,  $h_1 = 1.0$ ,  $Pr = 0.71$ ,  $h_2 = -1.0$ ,  $\theta_r = 0.2$ ,  $n = 0.5$ ,  $Sc = 0.66$ .



**Fig. 14.** Sherwood number distribution. (a)  $Sc$  with  $\varepsilon_2$  when  $\gamma = \tau = 0.1$  (b)  $\gamma$  with  $\tau$  where  $Sc = 0.66$ ,  $\varepsilon_2 = 0.1$  when  $\beta = 2$ ,  $M = Nr = \theta_s = Q = \varepsilon_1 = 0.1$ ,  $Gr = Gc = 0.05$ ,  $h_1 = 1.0$ ,  $Pr = 0.71$ ,  $h_2 = -1.0$ ,  $\theta_r = 0.2$ ,  $n = 0.5$ .

improving for greater Schmidt’s numbers. Fig. 14(b) depicts the variation of solute mass rate versus thermophoresis for a variation in chemical reaction parameters. For  $\gamma = 0.1$ , mass transfer coefficient is observed to grow linearly from 0.6788 to 0.8865, when the thermophoresis parameter varies from 0.1 to 1.0. For  $\gamma = 0.4$  the curve of mass transfer coefficient shows qualitatively a similar trend. Further higher values of  $\gamma$  improve the rate of mass transfer.

**5. Conclusions**

The objective of the current investigation is to report the flow characteristics of a MHD flow of a double stratified micropolar fluid considering non-linear thermal radiation, thermophoresis and second order wall slip. Due to the non-linear radiative heat transfer the energy equation is governed by the two temperature ratio parameters  $\theta_r$  and  $\theta_s$ . Some of the key findings of the present analysis are:

- Velocity has an increasing tendency throughout the boundary layer while microrotation has an opposite trend near the boundary and follows velocity in the rest of the region for increasing values of  $\beta$ ,  $Gr$  and  $Gc$ .
- Microrotation is seen to be dominant for larger values of  $\beta$  and  $n$ . Material parameter and both buoyancy parameters accelerate the flow.
- Thicker boundary layers are seen with larger absolute values of slip parameters.

- Non-linear thermal radiation serves as a boosting source of temperature.
- From a qualitative point of view, the temperature ratio parameters  $\theta_r$  and  $\theta_s$  have a contrast effect on temperature, that is, temperature enhances with increasing  $\theta_r$  while  $\theta_s$  does the reverse.
- Dual stratification parameters suppress the velocity.
- Thermal (solutal) stratification parameter drops the temperature (concentration) in the thermal (solutal) boundary layer.

**Acknowledgements**

The authors thank the reviewers for their constructive suggestions and valuable comments which led to a definite improvement in the paper.

**References**

Abo-Eldahab, M., Azzam, A., 2005. Thermal radiation effects on MHD flow past a semi-infinite inclined plate in the presence of mass diffusion. *Heat Mass Trans.* 41, 1056–1065.  
 Animasaun, I.L., 2017. Melting heat and mass transfer in stagnation point micropolar fluid flow of temperature dependent fluid viscosity and thermal conductivity at constant vortex viscosity. *J. Egypt. Math. Soc.* 25, 79–85.  
 Animasaun, I.L., Koriko, O.K., 2017. New similarity solution of micropolar fluid flow problem over an UHSPR in the presence of quartic kind of autocatalytic chemical reaction. *Front. Heat Mass Transfer* 8. <https://doi.org/10.5098/hmt.8.26>.

- Aurangzaib, Bhattacharyya, K., Shafie, S., 2016. Effect of partial slip on an unsteady MHD mixed convection stagnation point flow of a micropolar fluid towards a permeable shrinking sheet. *Alexandria Eng. J.* 55, 1285–1293.
- Batchelor, G.K., Shen, C., 1985. Thermophoretic deposition of particles in gas flowing over cold surfaces. *J. Colloid Interface Sci.* 107, 21–37.
- Cortell, R., 2014. Fluid flow and radiative nonlinear heat transfer over a stretching sheet. *J. King Saud Uni. Sci.* 26, 161–167.
- Crane, L., 1970. Flow past a stretching plate. *Z. Angew. Math. Phys.* 21, 645–647.
- Eluhu, C., Majumdar, D.R., 1998. Flow of a micropolar fluid through a circular cylinder subject to longitudinal and torsional oscillations. *Math. Comput. Model.* 27, 69–78.
- Eringen, A.C., 1966. Theory of micropolar fluids. *J. Math. Mech.* 16, 1–18.
- Fang, T., Yao, S., Zhang, J., Aziz, A., 2010. Viscous flow over a shrinking sheet with a second order slip flow model. *Commun Nonlinear Sci. Numer. Simul.* 15, 1831–1842.
- Fang, T., Zhang, Ji, Yao, S., 2009. Slip MHD viscous flow over a stretching sheet-An exact solution. *Com. Non. Sci. Numerical Sim.* 14, 3731–3737.
- Fukui, S., Kaneko, R., 1990. A Database for Interpolation of Poiseuille flow rates for high Knudsen number lubrication problems. *ASME J. Tribol* 112, 78–83.
- Gal-el-Hak, M., 1999. The fluid mechanics of micro-devices the freeman scholar lecture. *ASME Trans. J. Fluids Eng.* 121, 5–33.
- Geetanjali, C., Usha, R., Sahu, K.C., 2017. Core-annular miscible two-fluid flow in a slippery pipe: a stability analysis. *Phys. Fluids* 29, 097106.
- Ghosh, S., Usha, R., Sahu, K.C., 2014a. Linear stability analysis of miscible two-fluid flow in a channel with velocity slip at the walls. *Phys. Fluids* 26. <https://doi.org/10.1063/1.4862552>.
- Ghosh, S., Usha, R., Sahu, K.C., 2014b. Double-diffusive two-fluid flow in a slippery channel: a linear stability analysis. *Phys. Fluids* 26, 127101.
- Hayat, T., Ijaz Khan, M., Waqas, M., Alsaedi, A., Imran Khan, M., 2017a. Radiative flow of micropolar nanofluid accounting thermophoresis and Brownian moment. *Int. J. Hydrogen Energy* 42, 16821–16833.
- Hayat, T., Qasim, M., 2010. Influence of thermal radiation and joule heating on MHD flow of a Maxwell fluid in the presence of thermophoresis. *Int. J. Heat and Mass Trans.* 53, 4780–4788.
- Hayat, T., Ullah, S., Ijaz Khan, M., Alsaedi, A., Zaigham Zia, Q.M., 2018. Non-Darcy flow of water-based carbon nanotubes with nonlinear radiation and heat generation/absorption. *Results Phys.* 8, 473–480.
- Hayat, T., Zubair, M., Waqas, M., Alsaedi, A., Ayub, M., 2017b. On doubly stratified chemically reactive flow of Powell-Eyring liquid subject to non-Fourier heat flux theory. *Results Phys.* 7, 99–106.
- Hinds, W.C., 1982. *Aerosol Technology: Properties, Behaviour, and Measurement of Airborne Particles*. Wiley, New York.
- Ibrahim, W., 2017. MHD boundary layer flow and heat transfer of micropolar fluid past a stretching sheet with second order slip. *J. Braz. Soc. Mech. Sci. Eng.* 39, 791–799.
- Ibrahim, W., Makinde, O.D., 2013. The effect of double stratification on boundary-layer flow and heat transfer of nanofluid over a vertical plate. *Comput. Fluids* 86, 433–441.
- Ishak, A., Nazar, R., Pop, I., 2009. Boundary layer flow and heat transfer over an unsteady stretching vertical surface. *Meccanica* 44, 369–375.
- Karimipour, A., Orazio, A.D., Shadloo, M.S., 2017. The effects of different nano particles of  $Al_2O_3$  and Ag on the MHD nano fluid flow and heat transfer in a microchannel including slip velocity and temperature jump. *Physica E* 86, 146–153.
- Lukaszewicz, G., 1999. *Micropolar Fluids: Theory and Applications*. Birkhauser, Boston.
- Mabood, F., Ibrahim, S.M., Rashidi, M.M., Shadloo, M.S., Lorenzini, G., 2016. Non-uniform heat source/sink and sores effects on MHD non-Darcian convective flow past a stretching sheet in a micropolar fluid with radiation. *Int. J. Heat Mass Trans.* 93, 674–682.
- Makinde, O.D., 2011. MHD mixed-convection interaction with thermal radiation and  $n$ th order chemical reaction past a vertical porous plate embedded in a porous medium. *Chem. Eng. Comm.* 198, 590–608.
- Makinde, O.D., Animasaun, I.L., 2016a. Bioconvection in MHD nanofluid flow with nonlinear thermal radiation and quartic autocatalysis chemical reaction past an upper surface of a paraboloid of revolution. *Int. J. Thermo Sci.* 109, 159–171.
- Makinde, O.D., Animasaun, I.L., 2016b. Thermophoresis and Brownian motion effects on MHD bioconvection of nanofluid with nonlinear thermal radiation and quartic chemical reaction past an upper horizontal surface of a paraboloid of revolution. *J. Molecular Liquids* 221, 733–743.
- Mondal, H., Pal, D., Chatterjee, S., Sibanda, P., 2017. Thermophoresis and Soret-Dufour on MHD mixed convection mass transfer over an inclined plate with non-uniform heat source/sink and chemical reaction. *Ain Shams Eng. J.* Article in press.
- Pal, D., Chandra Das, B., Vajravelu, K., 2017. Influence of Non-linear Thermal Radiation on MHD double diffusive convection heat and mass transfer of a non-Newtonian fluid in a porous medium. *Int. J. Appl. Comp. Math.* 3, 3105–3129.
- Pande, G.C., Goudas, C.L., 1996. Hydromagnetic Rayleigh problem for a porous wall in slip flow regime. *Astrophys. Space Sci.* 243, 285–289.
- Rosca, N.C., Pop, I., 2013. Mixed convection stagnation point flow past a vertical flat plate with a second order slip: heat flux case. *Int. J. Heat Mass Transf.* 65, 102–109.
- Rosseland, S., 1931. *Astrophysik und Atom-Theoretische Grundlagen*. Springer Verlag, Berlin, pp. 41–44.
- Sahoo, B., Do, Y., 2010. Effects of slip on sheet-driven flow and heat transfer of a third grade fluid past a stretching sheet. *Int. comm. Heat and Mass Trans.* 37, 1064–1071.
- Sakiadis, B.C., 1961. Boundary layer behaviour on continuous solid surfaces: II. boundary layer on a continuous flat surface. *AIChEJ.* 7, 221–225.
- Sarojamma, G., Sreelakshmi, K., Vajravelu, K., 2018. Effects of dual stratification on non-orthogonal non-Newtonian fluid flow and heat transfer. *Int. J. Heat Technol.* 36, 207–214.
- Shadloo, M.S., Kimiaefar, A., Bagheri, D., 2013. Series solution for heat transfer of continuous stretching sheet immersed in a micropolar fluid in the existence of radiation. *Int. J. Numer. Meth. Heat Fluid Flow* 23, 289–304.
- Shah, N.A., Animasaun, I.L., Ibraheem, R.O., Babatunde, H.A., Sandeep, N., Pop, I., 2018. Scrutinization of the effects of Grashof number on the flow of different fluids driven by convection over various surfaces. *J. Molecular Liquids* 249, 980–990.
- Shateyi, S., 2013. A new numerical approach to MHD flow of a Maxwell fluid past a vertical stretching sheet in the presence of thermophoresis and chemical reaction. *Springer* 196, 1–14.
- Shidlovskiy, V.P., 1967. *Introduction to the Dynamics of Rarefied Gases*. American Elsevier publishing company, New York.
- Srinivasacharya, D., RamReddy, Ch., 2010. Heat and mass transfer by natural convection in a doubly stratified non-Darcy micropolar fluid. *Int. Comm. Heat and Mass Trans.* 37, 873–880.
- Srinivasacharya, D., RamReddy, Ch., 2011. Free convective heat and mass transfer in a doubly stratified non-Darcy micropolar fluid. *Korean J. Chem. Eng.* 28, 1824–1832.
- Talbot, L., Cheng, R.K., Schefer, R.W., Wills, D.R., 1980. Thermohoresis of particles in a heated boundary layer. *J. Fluid Mech.* 101, 737–758.
- Tsai, C.J., Lin, J.S., Aggarwal, S.G., Chen, D.R., 2004. Thermophoretic deposition of particles in laminar and turbulent tube flows. *Aerosol Science and Tech.* 38, 131–139.
- Wang, C.Y., 2002. Flow due to a stretching boundary with partial slip—an exact solution of the Navier-stokes equation. *Chem. Eng. Sci.* 57, 3745–3747.
- Waqas, M., Ijaz Khan, M., Hayat, T., Alsaedi, A., 2017. Stratified flow of an Oldroyd-B nanofluid with heat generation. *Results Phys.* 7, 2489–2496.
- Wu, L., 2008. A slip model for rarefied gas flows at arbitrary Knudsen number. *Appl. Phys. Lett.* 93, 253103–1–3.
- Yoshimura, A., Prudhomme, R.K., 1988. Wall slip corrections for couette and parallel disk viscometers. *J. Rheol.* 32, 53–67.